Semiconductor Science and Technology

PAPER • **OPEN ACCESS**

Strain engineering and strain measurement by spring tethers on suspended epitaxial GaN-on-Si photonic crystal devices

To cite this article: Jun Wang and Romuald Houdré 2024 *Semicond. Sci. Technol.* **39** 025010

OPEN ACCESS
IOP Publishing
Semiconductor Science and Technology
Semicond. Sci. Technol. **39** (2024) 025010 (6pp)
https://doi.org/10.1088/1361-6641/ad1b17

Strain engineering and strain measurement by spring tethers on suspended epitaxial GaN-on-Si photonic crystal devices

Jun Wang* **and Romuald Houdré**

Institute of Physics, École Polytechnique Fédérale de Lausanne (EPFL), Lausanne, Switzerland

E-mail: jun.wang@epfl.ch

Received 24 August 2023, revised 30 November 2023
Accepted for publication 4 January 2024
Published 23 January 2024

Abstract

Suspended epitaxial gallium nitride (GaN) on silicon (Si) photonic crystal devices suffer from large residual tensile strain, especially for long waveguides, because fine structures tend to crack due to large stress. By introducing spring-like tethers, designed by the combination of a spring network model and finite element method simulations, the stress at critical locations was mitigated and the cracking issue was solved. Meanwhile, the tethered-beam structure was found to be potentially a powerful method for high-precision strain measurement in tensile thin films, and in this case, a strain of $2.27(\pm 0.01) \times 10^{-3}$ was measured in 350 nm epitaxial GaN-on-Si.

Supplementary material for this article is available online

Keywords: GaN on Si, photonic crystal devices, strain engineering, strain measurement, tensile thin films.

1. Introduction

Photonic crystal (PhC) devices based on epitaxial gallium nitride (GaN) thin films on silicon (Si) (111) substrate are widely used for, e.g. nanophotonic applications, due to small light absorption and large transparent range [1–4]. These devices usually consist of a core part of PhC and a pair of waveguides for light coupling from the side of the chip. The PhC and the waveguides are suspended from the Si substrate in order to enable light confinement in the GaN film. Since the epitaxial GaN on Si exhibits residual tensile strain [5], the thin straight tethers that hold the waveguides tend to crack [1], which hampers the general application of the devices.

To solve the cracking issue, it is necessary to reduce the inner stress of the tethers, and here we propose two-dimensional spring-like tethers instead of straight tethers (figure 1). At constant deformation, the spring shape greatly reduces the inner stress of the tethers thanks to the large tether length. The spring shape also reduces the effective elastic constant of the tethers, resulting in more relaxation of the waveguides, larger deformation of the tethers, and larger inner stress of the tethers. However, this increase in inner stress is less effective than the reduction of inner stress by the large tether length, so, overall, the inner stress is still decreased.

Meanwhile, the tethered waveguide (beam) structure was found to be surprisingly effective for measuring the tensile strain. This is mainly because the waveguide (beam) is very long and is greatly relaxed so that the displacement at one of its endpoints is large and easy to measure.

* Author to whom any correspondence should be addressed.

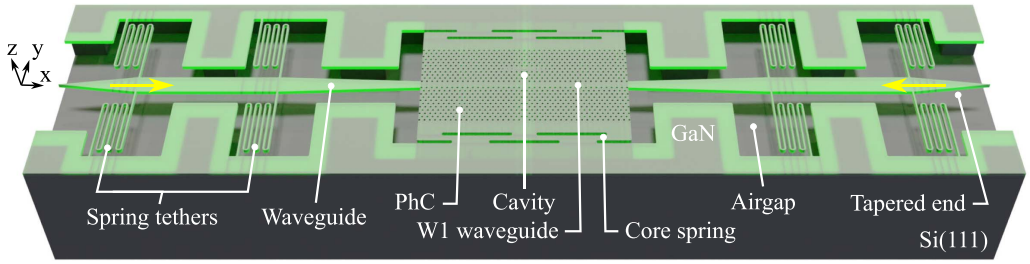

Figure 1. Schematic representation of a suspended GaN-on-Si photonic crystal device with spring tethers. Yellow arrows show the directions of movement when the waveguides are relaxed.

In this work, we show first that, the waveguide displacement and the maximum stress as a function of spring shape can be analyzed by a combination of a spring network model and finite element method (FEM) simulations. Then, we show that a group of devices with different spring shapes were fabricated and their endpoint displacements agree with the calculation results. Afterward, we show that the initial strain can be recalculated with high precision by using the measured displacements. Finally, we show that similar springs can be applied to the PhC part to avoid cracks.

2. Spring network model

Since there can be more than ten spring tether pairs attached to the long waveguide, the whole structure is too large for FEM simulation. To study the strain relaxation of the device, a spring network model is proposed (figures 2 (a) and (b)). The model assumes that the spring tethers and the waveguide are simple springs that are initially strained (attached to the substrate) and then relaxed (suspended) to reach a single stable state. The elastic constants of the springs are given by FEM simulations and used in the spring network model (figure 3(a)).

Due to the symmetry of the device, it is sufficient to take, e.g. the right side of the device as the network for analysis. The left side of the network is fixed, as well as the right side of each spring tether, while other parts are free to move. The joint points between spring tethers and the waveguide can be regarded as nodes, and there are the following relations:

$$0 = F_i^l + F_i^r + F_i^s, \tag{1}$$

$$F_i^s = -k_i^s \left(\delta x_i - \frac{\epsilon}{1+\epsilon} l_i^s \right), \tag{2}$$

$$F_i^l = -k_i \left(\frac{\epsilon}{1+\epsilon} l_i + \delta x_i - \delta x_{i-1} \right), \tag{3}$$

$$F_i^l = -F^r{}_{i-1}, \tag{4}$$

where F_i^l, F_i^r, and F_i^s are the forces applied to the ith node by the left waveguide segment, the right waveguide segment, and the spring tether pair, respectively; k_i^s and k_i are the elastic constants of the spring tether pair and the left waveguide segment, respectively; l_i^s and l_i are the initially strained width of the spring tether pair and the length of the left waveguide segment, respectively; ϵ is the initial strain; δx_i is the displacement of the ith node and it takes negative values. The boundary conditions for the spring network at the stable state after suspension are:

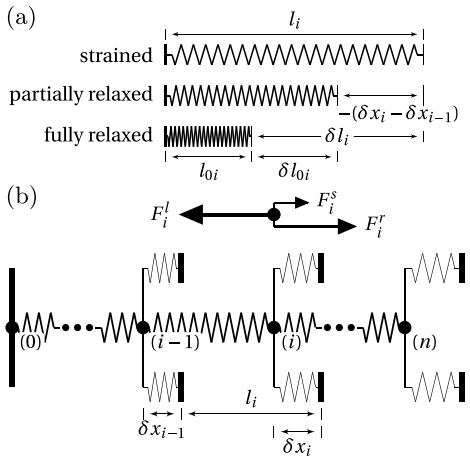

Figure 2. (a) Relations of a waveguide segment at different relaxation states. (b) Spring network of the right side of the device after suspension.

$$F_n^r = 0, \tag{5}$$

$$\delta x_0 = 0. \tag{6}$$

The equations above ultimately give the link among the initial strain ϵ, the node displacements δx_i, and the elastic constants k_i, k_i^s. The equations can be solved for the node displacements or the initial strain in an iterative way (see section 8 for details).

3. Spring tether simulations

To reduce the parameter space, the structure of the spring tether is mostly fixed, leaving the number of twists N and the main spring length L as free parameters (figure 3(b)). The width of the spring tether is 200 nm and the thickness is 350 nm. The inner round radius of the spring twist is 200 nm and the outer round radius is 400 nm. The corners at the joint between the tether and the waveguide (or the bulk film) are also rounded with a 200 nm radius to mitigate the local stress. The spring twists are optically isolated from the waveguide by a 2.0 μm gap.

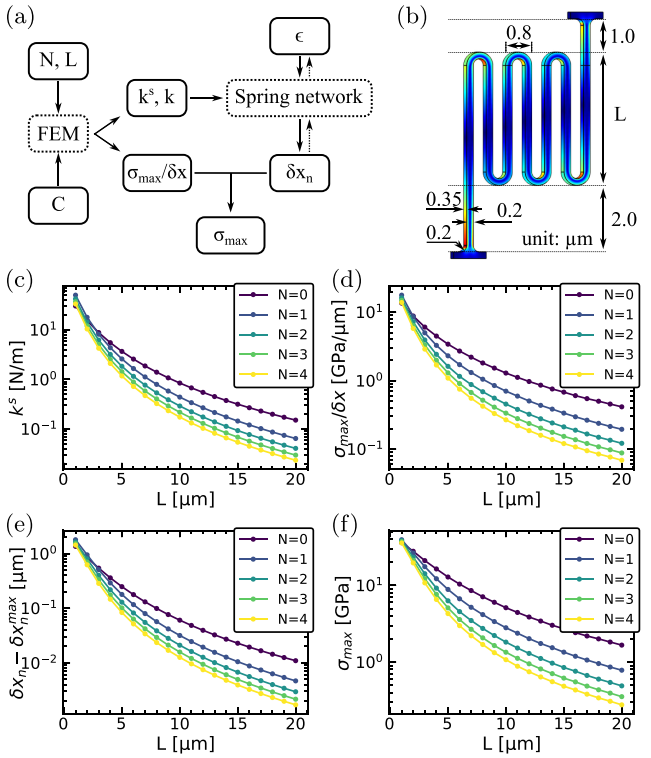

Figure 3. (a) Derivative relations among interested quantities: N, L, number of twists and main spring length; C, elastic matrix of GaN; FEM, finite element method; k^s, k, elastic constants of spring tether and waveguide segment; $\sigma_{\max}$, maximum stress in spring tethers; δx, deformation of spring tethers; ϵ, initial strain; δx_n, displacement of the last tether-waveguide joint. (b) Definition of spring dimensions. (c)–(f) Interested quantities as a function of spring shape N and L: (c) elastic constant along the waveguide direction k^s, from FEM simulation. (d) Maximum stress per unit deformation $\sigma_{\max}/\delta x$ in the spring tether, from FEM simulation. (e) Displacement of the last spring tether pair δx_n, from spring network calculation. (f) Maximum stress $\sigma_{\max}$ in the last spring tether.

The elastic constant of the spring tether pair along the waveguide direction (i.e. x-direction) k^s is given by FEM simulations (see section 8 for details) for combinations of N and L ($N = 0$ corresponds to straight tethers) (figure 3(c)). The maximum stress (usually at the tether-waveguide joint or in the twists) per unit deformation $\sigma_{\max}/\delta x$ is also given by FEM simulations (figure 3(d)).

Then, by assuming the initial strain $\epsilon = 2.52 \times 10^{-3}$ (see section 8 for details) and setting 10 pairs of spring tethers linearly spaced on a 1600 μm waveguide of 3 μm width and 350 nm thickness, the displacement of the last tether-waveguide joint δx_n is derived from the spring network model (figure 3(e)). A maximum displacement $\delta x_n^{\max} = -4.02\,\mu\text{m}$ can be expected when the elastic constants tend to zero. Finally, by multiplying the displacement δx_n and the maximum stress per unit deformation $\sigma_{\max}/\delta x$, the maximum stress in the spring $\sigma_{\max}$ is derived (figure 3(f)).

Need to mention that: (1) in terms of the spring tether thickness h, the elastic constant k^s is linearly dependent on h (as spring sheets in parallel) while the maximum stress $\sigma_{\max}$ is not dependent on h when the displacement is constant; (2) the displacement induced by the gravitational force is about four orders of magnitude smaller than the lateral displacement induced by strain and thus can be ignored; (3) the absolute displacement $|\delta x_n|$ and the maximum stress $\sigma_{\max}$ in the tethers can be reduced by adding more spring tether pairs, however, this will increase the force and stress in the waveguide and introduce more optical losses due to light scattering by the tethers.

4. Experimental test and analysis of spring tethers

The fabrication steps are as described in [1]. First, to estimate the stress at the breaking limit of the film, a preliminary test was carried out by introducing a small rectangular twist on the tethers. After suspension, some tethers at the breaking limit were captured by scanning electron microscope (SEM) and a lateral displacement of about 0.2 μm is measured (figure 4(a)). According to the curvature radius seen on the SEM image, the critical stress at tether breaking can be estimated to be about 10 GPa, which is in agreement with Vickers hardness measurements [6].

Then, devices with different spring tether shapes (N and L) and repetition periods (l) are fabricated. Examples are given for a group of devices each with 10 pairs of spring tethers linearly spaced on a waveguide of 1570 μm total length, 3 μm width, and 350 nm thickness. PhCs with 60 μm width and 15 μm height are located at the center of the devices. SEM images of the last spring tether pair are shown for four devices on the same chip with the number of twist $N = 3$ and the main spring length L equals to 4 μm, 8 μm, 12 μm, and 16 μm, respectively (figure 4(b)). The tethers on device 1 are broken due to large stress in the spring. The last tether pair displacement δx_n^* of devices 2–4 can be measured by digital image processing (see section 8 for details) as −3.57 μm, −3.57 μm and −3.54 μm, respectively (table 1). Both simulations and experiments show that δx_n for devices 2–4 are close to each other, which is due to the fact that the spring tethers are soft and the displacements are close to the maximum value. The difference between simulated and experimental displacements mainly comes from the uncertainty of the initial strain and material stiffness. Compared to short straight tethers (table 1 (device 5–6)), the spring tethers help to reduce the maximum stress in tethers by about 1 order of magnitude and the maximum force in the waveguide by about 2 orders of magnitude.

5. Strain measurement by tethered beam

When the displacement δx_n is measured by digital image processing on the SEM images, the initial strain ϵ can be derived through the spring network model. By using the measured δx_n^*, the initial strain ϵ^* derived for devices 2-4 are 2.28×10^{-3}, 2.28×10^{-3} and 2.26×10^{-3}, respectively (table 1), from which a variation of 1×10^{-5} can be estimated. This provides an experimental method to measure the film strain, i.e. measure the displacement of the last tether-waveguide joint and then calculate the initial strain through the spring network model.

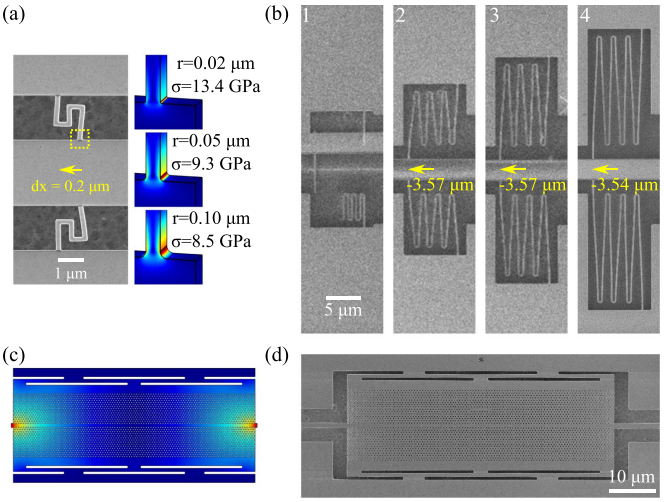

Figure 4. (a) Scanning electron microscope (SEM) image of a pair of one-twist square spring tethers at critical deformation. Insets on the right side show the finite element method (FEM) simulations for maximum stress σ with three different estimations of corner round radius r (yellow box). (b) SEM images of the last spring tether pairs (node n) on four devices on the same chip after suspension, with $N = 3$ and L equals to 4, 8, 12, 16 μm, respectively. (c) Photonic crystal (PhC) under stretching force by the waveguides. Colormap shows the total displacement. (d) SEM image of the springs around the PhC slab.

Table 1. Quantities from simulation and experiment for different devices. l is the average distance between two adjescent tether pairs, δx_n is the displacement of the last tether pair, $\sigma_{\max}$ is the maximum stress in the tether, $F_{\max}$ is the maximum force in the waveguide. δx_n, $\sigma_{\max}$, and $F_{\max}$ are given by simulation assuming the initial strain $\epsilon = 2.52 \times 10^{-3}$. δx_n^* is the displacement measured on SEM images, and ϵ^* is the initial strain calculated from δx_n^*.

Device	N	L (μm)	l (μm)	δx_n (μm)	$\sigma_{\max}$ (GPa)	$F_{\max}$ (μN)	δx_n^* (μm)	ϵ^* ($\times 10^{-3}$)
1	3	4	150	−3.78	7.53	52.09	–	–
2	3	8	150	−3.93	2.04	8.77	−3.57	2.28
3	3	12	150	−3.95	0.94	2.83	−3.57	2.28
4	3	16	150	−3.96	0.54	1.24	−3.54	2.26
5	0	1	150	−2.59	38.76	378.0	–	–
6	0	1	20	−1.14	16.99	669.0	–	–

There are some good features of this method compared to other methods [7–9]: (1) The derived initial strain ϵ is not dependent on the stiffness values used in FEM simulations. This is because the errors on ϵ induced by the waveguide (beam) segment elastic constants k_i and by the tether spring elastic constant k_i^s compensate each other. (2) The derived initial strain ϵ (or displacement δx_n) is not sensitive to k_i^s (nor to k_i) when k_i^s is much smaller than k_i. For example, on devices 1–4, 10% error of k_i^s (or k_i) results in only about 0.46%, 0.08%, 0.02% and 0.01% error of ϵ, respectively. (3) The accuracy of the derived initial strain ϵ can be very high. This is because the beam is almost fully relaxed and can be very long, thus the displacement of the last tether-waveguide joint can be large and easy to measure. The insensitivity to elastic constant errors also contributes. Digital image processing on high-resolution SEM images and further improves the accuracy. Notice that, a bare beam without tethers may not work since the beam may bend out of the film plane. (4) The tethered beam is fully on-chip and can be fabricated simultaneously with other devices through the same microfabrication processes.

6. Spring around PhC

Springs can also be applied to the PhC part, where the stress of concern is mainly in the direction perpendicular to the waveguides (i.e. y-direction). Different from the tethers for the waveguide, the springs for the PhC part are designed to be soft in the y-direction and rigid in the x-direction in case the forces applied by the waveguides are not balanced, which results in a shape as ribs with 0.8 μm width. The resulting corners are also rounded with 0.2 μm width radius. FEM simulations show that the effective elastic constant of the upper half of the springs in the y-direction is $1.8 \times 10^2\,\mathrm{Nm}^{-1}$, much smaller than that of the upper half of the PhC, $3.5 \times 10^5\,\mathrm{Nm}^{-1}$, which ensures that the deformation under stretch is mainly absorbed by the spring. The effective elastic constant of the right half of the springs (both up- and down-side parts) in the x-direction is $2.9 \times 10^4\,\mathrm{Nm}^{-1}$, which is comparable to that of the right side of the PhC (with force only applied at the joint part with the waveguide), $2.0 \times 10^4\,\mathrm{Nm}^{-1}$. The effective elastic constant of the right half of the PhC attached to the springs in the x-direction is $2.0 \times 10^4\ \mathrm{Nm}^{-1}$, same as that of the PhC alone, which transforms to 50 nm displacement with 1.0×10^{-3} N force from the waveguides (figure 4(c). This implies that, when short straight tethers are applied to the waveguides, the large force at the waveguide-PhC joints may induce a deformation of the geometry and a modification of the refractive index that changes the optical design for light coupling. With spring tethers applied to the waveguides, the maximum displacement at the waveguide-PhC joint should be reduced to the sub-nanometer range, which is an additional benefit of the spring tethers.

PhCs with springs were fabricated together with the spring-tethered waveguides (figure 4(d)). SEM images show that all PhCs maintained their shape without cracks and no obvious deformation was observed as expected.

7. Discussions and conclusions

Although the simulated values of elastic constant, inner stress, and force presented above are not calibrated because of the difficulties in measurements of these quantities, they provide an order of magnitude for comparison and agree with the cracking behavior in experiments. The accuracy of the derived displacements or initial strain is not sensitive to the accuracy of the elastic constants from FEM simulations, as long as the tethers are much softer than the waveguide segment, which is an advantage of the tethered-beam structure. Compared to straight tethers, the spring tethers provide the following benefits: (1) the inner stress in the tethers is reduced and the stability of the device is improved; (2) stable devices are enabled with fewer tether pairs so that optical losses due to scattering are reduced; (3) deformation at the waveguide-PhC joint is reduced so that the light coupling between waveguide and PhC is improved. Need to mention that the spring tethers add no more complexity in microfabrication because the springs are 2D and in the same layer as the waveguide, so the lithography and the etching steps are the same as for devices with straight tethers.

To conclude, firstly, the spring tethers and the springs around PhCs successfully solved the cracking issue of the suspended GaN-on-Si PhC devices. Compared to short straight tethers, the spring tethers attached to the waveguides reduce the maximum stress in tethers by 1 order of magnitude and the maximum force in waveguides by 2 orders of magnitude. The spring tethers also help to reduce the total number of tethers and the deformation at the waveguide-PhC joint, adding benefits to optical aspects. Secondly, the suspended tethered-beam structure can also be used to measure the initial strain in tensile thin films with high precision, and as a demonstration, a strain of $2.27(\pm 0.01) \times 10^{-3}$ was measured in 350 nm epitaxial GaN-on-Si here.

8. Methods

In the spring network model, when the initial strain ϵ and the elastic constants are known, the node displacement δx_n can be derived numerically by the following steps:

1. assign an estimated value to δx_n;
2. calculate F_n^l by applying equations (1), (2) and (5) at node n;
3. calculate δx_{n-1} and F_{n-1}^r by applying equations (3) and (4) at node n;
4. calculate δx_1 (note as $\delta x_{1,1}$) by repeating steps 2 and 3 for nodes $n-1, n-2, \ldots, 1$;
5. calculate δx_1 (note as $\delta x_{1,2}$) by applying equations (3) and (6) at node 1;
6. calculate $\Delta(\delta x_n) = |\delta x_{1,1} - \delta x_{1,2}|$;
7. repeat the steps above and find the solution of δx_n with a desired accuracy by minimizing $\Delta(\delta x_n)$.

Since the system is linear, $\Delta(\delta x_n)$ has one single minima as zero. Step 7 can be efficiently done by optimization methods, e.g. golden-section search. Conversely, when the node displacement δx_n is known, the initial strain ϵ can be calculated by adding another optimization layer on top of the above steps.

The FEM simulations are done with COMSOL Multiphysics® (Solid Mechanics interface). The film is considered linearly elastic and the elastic matrix of wurtzite GaN can be expressed as [10]:

$$C = \begin{bmatrix} C_{11} & C_{12} & C_{13} & 0 & 0 & 0 \\ C_{12} & C_{11} & C_{13} & 0 & 0 & 0 \\ C_{13} & C_{13} & C_{33} & 0 & 0 & 0 \\ 0 & 0 & 0 & C_{44} & 0 & 0 \\ 0 & 0 & 0 & 0 & C_{44} & 0 \\ 0 & 0 & 0 & 0 & 0 & (C_{11} - C_{12})/2 \end{bmatrix}, \quad (7)$$

where stiffness elements $C_{11} = 390\,\text{GPa}$, $C_{12} = 145\,\text{GPa}$, $C_{13} = 106\,\text{GPa}$, $C_{33} = 398\,\text{GPa}$, $C_{44} = 105\,\text{GPa}$ for bulk crystal [11, 12]. Young's modulus $E_x = E_y = 324\,\text{GPa}$ and $E_z = 356$ GPa can be derived from the elastic matrix for manual calculations. Gallium nitride (GaN) density $\rho_{\text{GaN}} = 6.15 \times 10^3\,\text{kg m}^{-3}$ [13] can be used for gravitational force calculation. In the GaN-on-Si sample, there is also a thin (about 30–40 nm) aluminium nitride (AlN) buffer layer to prevent reaction between GaN and Si. Since the AlN buffer layer is very thin, it is considered the same as GaN in the simulations.

The initial strain $\epsilon = 2.52 \times 10^{-3}$ is estimated by considering the thermal mismatch between GaN and Si(111) substrate. For a beam of epitaxial Ga-on-Si, the GaN film is attached to the Si substrate and they have the same length at the growth temperature, so we have $L_{\text{Si}}^{T1}(a_{\text{Si}}^{T2}/a_{\text{Si}}^{T1}) = L_{\text{GaN}}^{T1}(a_{\text{GaN}}^{T2}/a_{\text{GaN}}^{T1})$, where $T1 = 300\,\text{K}$ is the room temperature, $T2 = 1300\,\text{K}$ is the growth temperature, L_{Si}^{T1} and L_{GaN}^{T1} are the free standing lengths of Si and GaN at the room temperature, respectively, $a_{\text{Si}}^{T1} = 5.431/\sqrt{2}$ Å [14], $a_{\text{Si}}^{T2} = 5.453/\sqrt{2}$ Å [14], $a_{\text{GaN}}^{T1} = 3.189$ Å [15], and $a_{\text{GaN}}^{T2} = 3.210\,\text{Å}$ [15] are lattice constants of Si and GaN at the room temperature and at the growth temperature, respectively. Then, the film strain at the room temperature before suspension can be calculated by $\epsilon_{\text{GaN}}^{T1} = (L_{\text{Si}}^{T1} - L_{\text{GaN}}^{T1})/L_{\text{GaN}}^{T1} = (a_{\text{GaN}}^{T2}/a_{\text{GaN}}^{T1})(a_{\text{Si}}^{T1}/a_{\text{Si}}^{T2}) - 1$. This estimation is rough since the lattice mismatch also contributes to strain, nevertheless, it provides an initial guess of the strain value prior to experiments.

The spring displacements δx_n^* on devices 2–4 are measured by analyzing the SEM images. Profiles are extracted along horizontal lines across the images and the features are fitted to get the positions with subpixel precision. For instance, the tethers are fitted with Gaussian functions and the edges of the air gaps are fitted with Sigmoid functions. The lateral widths of the air gaps and tether springs before suspension are 9.2 μm and 3.6 μm, respectively, for devices 1–4.

Data availability statement

All data that support the findings of this study are included within the article (and any supplementary files).

Acknowledgments

This work was supported by the Swiss National Science Foundation, through Projects Numbers 200020-169590 and 200020-188649. The authors would like to acknowledge Dr Jean-François Carlin and Prof. Nicolas Grandjean from the Laboratory of Advanced Semiconductors for Photonics and Electronics (LASPE) for providing the GaN-on-Si wafers.

ORCID iDs

Jun Wang https://orcid.org/0000-0001-8406-1537
Romuald Houdré https://orcid.org/0000-0003-3348-506X

References

[1] Vico Trivi no N, Dharanipathy U, Carlin J-F, Diao Z, Houdré R and Grandjean N 2013 *Appl. Phys. Lett.* **102** 081120
[2] Mohamed M S, Simbula A, Carlin J-F, Minkov M, Gerace D, Savona V, Grandjean N, Galli M and Houdré R 2017 *APL Photonics* **2** 031301
[3] Wang J, Clementi M, Minkov M, Barone A, Carlin J-F, Grandjean N, Gerace D, Fan S, Galli M and Houdré R 2020 *Optica* **7** 1126
[4] Butté R and Grandjean N 2020 *Nanophotonics* **9** 569
[5] Dadgar A 2015 *Phys. Status Solidi* b **252** 1063
[6] Yonenaga I 2002 *MRS Internet J. Nitride Semicond. Res.* **7** 1
[7] Bhowmick S, Espinosa H, Jungjohann K, Pardoen T and Pierron O 2019 *MRS Bull.* **44** 487
[8] Cuddalorepatta G K, Li H, Pantuso D and Vlassak J J 2020 *Materialia* **9** 100502
[9] Grachev S, Hérault Q, Wang J, Balestrieri M, Montigaud H, Lazzari R and Gozhyk I 2022 *Nanotechnology* **33** 185701
[10] Butté R and Grandjean N 2008 *Polarization Effects in Semiconductors: From Ab Initio Theory to Device Applications* (Springer) pp 476–476
[11] Polian A, Grimsditch M and Grzegory I 1996 *J. Appl. Phys.* **79** 3343
[12] Vurgaftman I and Meyer J R 2003 *J. Appl. Phys.* **94** 3675
[13] Levinshtein M E, Rumyantsev S L and Shur M S 2001 *Properties of Advanced Semiconductor Materials: GaN, AIN, InN, BN, SiC, Sige* (Wiley)
[14] Okada Y and Tokumaru Y 1984 *J. Appl. Phys.* **56** 314
[15] Roder C, Einfeldt S, Figge S and Hommel D 2005 *Phys. Rev.* B **72** 085218